Thermal expansion and anharmonicity of solid Kr studied by extended x-ray-absorption fine structure

Toshihiko Yokoyama and Toshiaki Ohta
Department of Chemistry, Graduate School of Science, The University of Tokyo, 7-3-1 Hongo, Bunkyo-ku, Tokyo 113, Japan

Hitoshi Sato
Department of Materials Science, Faculty of Science, Hiroshima University, 1-3-1 Kagamiyama, Higashi-Hiroshima, Hiroshima 739, Japan

(Received 7 November 1996; revised manuscript received 8 January 1997)

Kr *K*-edge extended x-ray-absorption fine-structure spectra of solid Kr were measured over the temperature range of 24–43 K. The thermal expansion and Debye temperature were obtained by the analysis of the first-, third-, and fourth-nearest-neighbor (NN) Kr-Kr shells. For the third- and fourth-NN shells, the conventional Gaussian-distribution approximation was found to give the proper thermal expansion. On the other hand, for the first-NN shell, the cumulant-expansion analysis including the third-order asymmetry of the distribution function is necessary, although the higher-NN shells are more largely disordered in terms of the mean-square relative displacements. These results were confirmed by the classical Monte Carlo simulations. Effective cancellation of the asymmetric contribution was thus clarified for the higher-NN shells. The quantum-statistical calculations of the first-NN cumulants of Kr clusters were also carried out by varying the cluster size in order to examine the relationship between the pair potential and observed cumulants, and to justify the employed Kr-Kr pair potential. [S0163-1829(97)14917-7]

I. INTRODUCTION

Thermal expansion is one of the direct measures of anharmonicity in molecules and solids. Since the interatomic potential is generally asymmetric with respect to the potential minimum, the average interatomic distance is temperature dependent and usually increases with a temperature rise because of a looser barrier at a longer distance side. Extended x-ray-absorption fine-structure (EXAFS) spectroscopy gives information on local thermal expansion and anharmonicity for solids,[1–4] molecules,[5–7] and noncrystalline materials[2] owing to the establishment of the cumulant-expansion technique.[8] Very recently, the relationship between the EXAFS cumulants and the anharmonic interatomic potential has also been clarified,[3,5–7,9–11] including many-atom systems[5–7,10,11] and many-body forces.[6,7]

Since thermal expansion originates from anharmonicity of a pair potential, it happens to be believed that, when the asymmetric distribution is neglected in the EXAFS analysis by assuming the Gaussian distribution function, thermal expansion cannot be estimated and the obtained distance is erroneously getting shorter with a temperature rise.[12] The third-order cumulant which describes the mean-cubic relative displacement (degree of asymmetric distribution) should be taken into account in order to estimate appropriate temperature dependence of the average distance. Very recently, however, Di Cicco *et al.*[13] have investigated EXAFS spectra of solid and liquid Kr under high pressure at room temperature, and remarked that asymmetry of the distribution functions for higher-nearest-neighbor (NN) Kr-Kr shells can be neglected, while it should be taken into account for the first-NN shell. Although this assumption was confirmed by their classical Monte Carlo (MC) simulations, they did not address the finding in detail since their main purpose was to account for the structural and vibrational properties at high pressure.

This remark given by Di Cicco *et al.*[13] is quite interesting, because usually higher-NN shells without direct interactions between the atom pairs show larger disorder. Actually, they found that the mean-square relative displacement is larger for higher-NN shells than for the first-NN one. If this is commonly true, the EXAFS formula can be significantly simplified and thermal expansion is appropriately estimated without taking the asymmetry of the radial distribution function into account. In the present study, we have thus investigated EXAFS of solid Kr at low temperature in order to clarify their remark by analyzing the first- and higher-NN Kr-Kr shells. The thermal expansion of solid Kr is large enough to estimate within the errors of EXAFS in rather a narrow temperature range. The vibrational properties have subsequently been simulated using a classical Monte Carlo simulation according to the manner by Di Cicco *et al.*,[13] in order to explain the present experimental results.

The other purpose in the present study is to carry out analytical quantum-statistical calculations of the EXAFS cumulants of solid Kr. In our previous studies, we have investigated simple molecules of linear,[5] tetrahedral,[6] and octahedral[7] MX_n ($n=3,4,6$) systems. In such cases, the cumulants of the first-NN shells are not so different from those given by assuming a simple two-body Einstein system, since there exist chemical bonds only for the M-X pairs without direct X-X interactions. Thus we have paid our attention mainly to higher-NN shells by taking not only the stretching force constants, but also the bending modes into account. On the other hand, solid Kr shows fcc structure, in which the first-NN Kr atoms surrounding the central (x-ray-absorbing) Kr have also the first-NN interactions with each other. It is worthwhile investigating the EXAFS cumulants by varying

the size of Kr clusters. It should also be noted that solid Kr is a suitable example since its solid-state property is described within a two-body interatomic potential (many-body forces can be ignored) and that a temperature-dependent EXAFS study of solid Kr has never been reported in spite of fundamental noble-gas systems.

The present paper is described in the following sequence. After experimental details are briefly given in Sec. II, the EXAFS spectra are analyzed in Sec. III mainly to obtain the temperature dependence of the cumulants. The Debye temperature and the thermal expansion are consequently determined in this section. Section IV deals with the classical MC simulations, by which the asymmetry of the radial distribution functions of the first- and higher-NN shells is clarified. In Sec. V, the analytical quantum-statistical calculations of the cumulants are described. We will show the cluster-size dependence of the cumulants for the first-NN shell. Section VI gives concluding remarks of the present investigation.

II. EXPERIMENTAL DETAILS

Kr K-edge EXAFS spectra of solid Kr were measured at BL-10 B (Ref. 14) of the Photon Factory in the National Laboratory for High Energy Physics (KEK-PF, the ring operation energy of 2.5 GeV and stored current of 350–250 mA) with the transmission mode using a Si(311) channel-cut monochromator. Ionization chambers were employed for the measurement of intensities of incident (I_0) and transmitted (I) x rays. Data acquisition time was 1 s for each data point. Commercially available high-purity Kr gas was condensed on an Al foil (15 μm) at 24 K. The Kr K-edge absorption jump was found to be 0.9. EXAFS spectra were taken at 24, 25, 29, 35, 38, and 43 K. No desorption of Kr was detected during the EXAFS measurements judging from the edge jump, and abrupt desorption took place at 45 K. Temperatures were monitored with a calibrated Si diode attached to the Al foil. The accuracy of temperature was estimated to be less than ± 1 K.

III. EXAFS

A. Reduction of experimental data

In order to extract reliable EXAFS oscillation functions $\chi(k)$ (k is the photoelectron wave number), the atomic background originating from the double-electron excitation processes was subtracted from the raw EXAFS spectra according to the method proposed by Di Cicco *et al.*[13] The background-corrected spectra were analyzed with well-established procedures: post-edge background subtraction using cubic-spline polynomials and subsequent normalization with the absorption coefficients given in the literature.[15,16] The inflection point of the Kr K edge at 24 K was tentatively chosen as the edge energy E_0. The temperature dependences of the extracted EXAFS oscillation functions $k^3\chi(k)$ are resultantly shown in Fig. 1(a).

The EXAFS functions obtained were subsequently Fourier transformed into r space ($\Delta k_{\mathrm{FT}}=3.2-10.4$ Å^{-1}), these being depicted in Fig. 1(b). The magnitude of the Fourier transform is clearly found to decrease with the temperature rise. It is noted that when the double-electron excitations are not taken into account for the extraction of $\chi(k)$, a strong

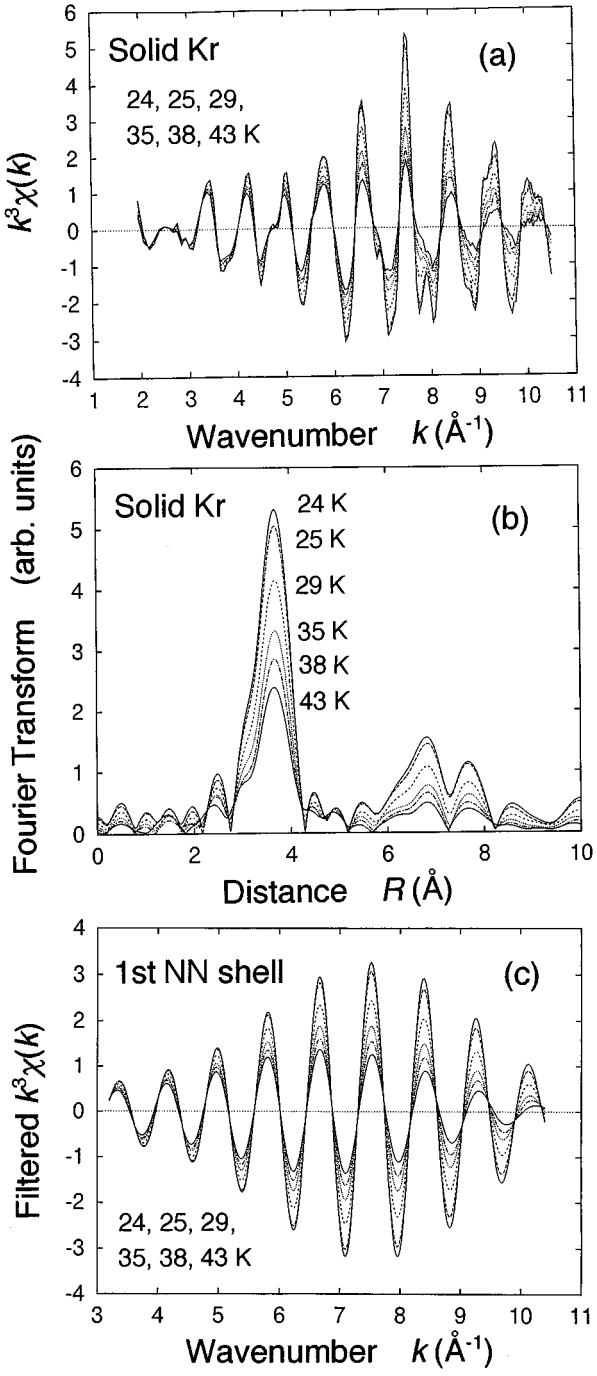

FIG. 1. (a) Kr K-edge EXAFS oscillation functions $k^3\chi(k)$ of solid Kr at 24, 25, 29, 35, 38, and 43 K, where the contribution of double-electron excitations were subtracted; (b) Fourier transforms of (a) using the Fourier range of $\Delta k_{\mathrm{FT}}=3.2-10.4$ Å^{-1}; (c) filtered $k^3\chi(k)$ for the first-NN shell using the Fourier ranges of $\Delta k_{\mathrm{FT}}=3.2-10.4$ Å^{-1} and $\Delta R=2.9-4.2$ Å^{-1}.

peak emerges at a short-distance region. Since solid Kr shows a fcc structure, the assignments of the Fourier peaks are straightforward. The first-NN shell (coordination number $N=12$) appears at $\sim$3.7 Å, while the third-NN ($N=24$) and fourth-NN ($N=12$) shells are found at $\sim$6.9 and $\sim$7.5 Å, respectively. The second-NN shells are not explicitly seen in the Fourier transforms even at the lowest temperature of 24 K, probably because the coordination number is compara-

tively small ($N=6$) and the mean-square relative displacement (the EXAFS Debye-Waller factor) is larger than those for the other shells. The fourth-NN shell is known to contain the multiple-scattering path because of the collinear configuration in fcc solids. The filtered $k^3\chi(k)$ for the first-NN shell ($\Delta k_{\rm FT}=3.2-10.4$ Å^{-1} and $\Delta R=2.9-4.2$ Å) are depicted in Fig. 1(c). One can obviously find the amplitude reduction and phase delay at higher temperatures, which originate from the enhancements of the mean-square and cubic relative displacements, respectively.

B. Analysis of the lowest-temperature data

The lowest-temperature data were at first analyzed. In order to obtain the scattering amplitudes and phase shifts, we performed FEFF6 (Ref. 17) calculations of a Kr_{55} ($KrKr_{12}Kr_6Kr_{24}Kr_{12}$) cluster for the temperature of 24 K. Here the interatomic distance R was referred to from the literature,[18] and the values of the mean-square relative displacement C_2 were estimated by assuming the correlated Debye model[19] using the Debye temperature $\Theta_D=61$ K (see below). The mean-cubic relative displacement C_3 was neglected. The remaining two variables of S_0^2 (the intrinsic loss factor) and ΔE_0 (edge energy shift) were roughly optimized to be 1.35 and -0.8 eV, respectively. Although S_0^2 of 1.35 seems a little too large, this is partly because in the present experimental spectra the double-electron excitation contributions were subtracted in advance from the raw spectra. Figure 2 shows the FEFF6 results, together with the experimental data at 24 K. The FEFF6 calculation was found to reproduce up to the fourth-NN shell fairly well. Especially, as found in the experimental Fourier transform, the second-NN shell was not seen well also in the theoretical one. The obtained Fourier transform of the FEFF6 spectrum was Fourier filtered for the shell of interest to derive the scattering amplitudes in a similar manner to the experimental data.

For the third- and fourth-NN shells, these two contributions were slightly superposed with each other, as seen in the experimental data of Fig. 2(b). In order to distinguish these two contributions, FEFF6 calculations were performed separately; for the third-NN shell, the EXAFS function originating only from the first- and third-NN shells was first calculated and then Fourier filtered, while for the fourth-NN shell, the EXAFS function originating only from the first- and fourth-NN shells was similarly calculated and Fourier filtered. Although the FEFF6 calculation of the Kr cluster automatically yields each backscattering amplitude and phase shift separately, these functions might not directly be compared with the Fourier-filtered experimental EXAFS spectra because of the truncation effects in the Fourier transformation. In order to reduce the artificial effects, it seems better to perform similar treatments of the Fourier and inverse Fourier transforms for the theoretical standard as well.

It is also noted that the fourth-NN shell contains five different kinds of the scattering path; three of them correspond to collinear paths [Kr^0-Kr^{IV}-Kr^0 (single scattering), Kr^0-Kr^I-Kr^{IV}-Kr^0 (double), and Kr^0-Kr^I-Kr^{IV}-Kr^I-Kr^0 (triple), where the x-ray-absorbing Kr^0, the first-NN Kr^I, and the fourth-NN Kr^{IV} are located collinearly], and the remains two consist of twice-backscattering paths [Kr^0-Kr^I-Kr^0-Kr^I-Kr^0 and Kr^0-Kr^I-Kr^0-$Kr^{I'}$-Kr^0 (triple scattering)]. The last two paths were found to be essentially weak and are negligible. This implies that the scattering amplitude obtained by the Fourier filtering for the fourth-NN shell is the averaged one among the three collinear inequivalent paths. This approximation is meaningful as long as the dynamical effect of the scattering amplitude is negligible,[20] since the C_2 and C_3 values should be all equal in these three paths.[5,7]

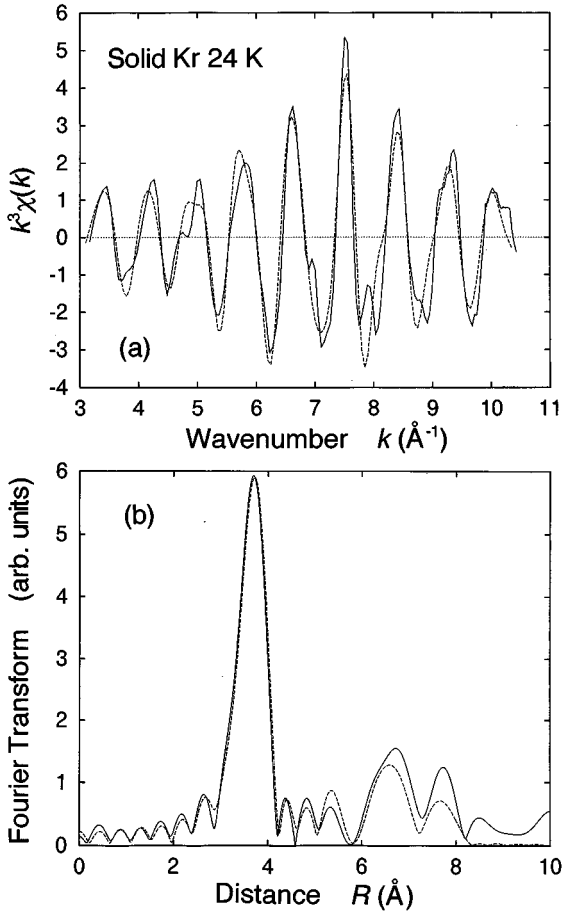

FIG. 2. (a) Kr K-edge EXAFS oscillation functions $k^3\chi(k)$ and (b) their Fourier transforms of solid Kr at 24 K obtained by the FEFF6 calculation (dashed line), together with the experimental data.

The curve-fitting analysis was performed for the first-, third-, and fourth-NN shells. For the first-NN shell, the one-shell analysis can be applied by employing the ranges of $\Delta k_{\rm FT}=3.2-10.4$ Å^{-1}, $\Delta R=2.9-4.2$ Å, and $\Delta k_{\rm fit}=4-10$ Å^{-1} (the number of independent data points, $N_{\rm ind}\sim 6$). For the third- and fourth-NN shells, the two-shell fitting was performed by using the ranges of $\Delta k_{\rm FT}=3.2-10.4$ Å^{-1}, $\Delta R=5.8-8.2$ Å, and $\Delta k_{\rm fit}=4-10$ Å^{-1} ($N_{\rm ind}\sim 10$). In both fitting procedures we used S_0^2, the interatomic distance R, the edge-energy shift ΔE_0, and C_2 as fitting parameters. Since S_0^2 and ΔE_0 were allowed to vary depending on the shell, the numbers of fitting parameters were thus 4 and 8 for the analyses of the first- and higher-NN (third- and fourth-NN) shells, respectively. The obtained results are summarized in Table I. The interatomic distances are found to be in excellent agreement with the x-ray data[18] for all the shells, although corrections due to C_2 and C_3 discussed below were neglected in these fittings. As men-

TABLE I. Structural parameters of the first-, third-, and fourth-NN shells of solid Kr at 24 K given by FEFF6 (Ref. 17). The interatomic distance R in parentheses corresponds to the x-ray diffraction data (Ref. 18), and those for C_2 are the calculated ones using the correlated Debye model ($\Theta_D = 61$ K). The errors of data and fits are roughly estimated from the change of the residual factors to be 10–20% for S_0^2, $\pm 0.25\%$ for R, and $\pm 10\%$ for C_2. No ambiguities of the theoretical standards are included.

Shell	S_0^2	R (Å)	C_2 (10^{-2} Å^2)
First	1.3	3.990 (4.0019)	1.57 (1.76)
Third	1.2	6.943 (6.9314)	1.85 (2.19)
Fourth	1.8	8.012 (8.0037)	2.17 (2.20)

tioned above, the S_0^2 values were again overestimated, partly because of the subtraction of the double-electron excitation contributions in advance. On the other hand, it is rather surprising that the absolute values of C_2 also show good agreement with the correlated Debye model, in spite of the fact that only the temperature dependence of C_2 may often be meaningful.

C. Analysis of the temperature dependence

The temperature dependence was subsequently analyzed. In order to discuss small differences of the interatomic distance, let us here carefully define the EXAFS formula of a single shell within the fourth-order cumulant-expansion technique as

$$\chi(k) = A(k)\sin\Phi(k),$$

$$A(k) = A_0(k)\exp[-2C_2k^2 + \tfrac{2}{3}C_4k^4],$$

$$\Phi(k) = 2k\left[R_{\rm av} - C_2\left(\frac{1}{R_{\rm av}} + \frac{2}{\lambda}\right)\right] - \frac{4}{3}C_3k^3 + \phi(k), \quad (1)$$

where $A_0(k)$ is the temperature-independent part of the amplitude, $\phi(k)$ the total phase shift, and λ the mean free path of the photoelectron (here $\lambda = 10$ Å was assumed). The distance $R_{\rm av}$ and ith-order cumulants C_i are given as thermal averages such that $R_{\rm av} = \langle r \rangle$, $C_2 = \langle (r - R_{\rm av})^2 \rangle$, $C_3 = \langle (r - R_{\rm av})^3 \rangle$, and $C_4 = \langle (r - R_{\rm av})^4 \rangle - 3C_2^2$ ($\langle\ \rangle$ denotes the thermal average). In the equation of $\Phi(k)$, the correction term of the distance, $C_2(1/R_{\rm av} + 2/\lambda)$, is slightly different from that given by Tranquada and Ingalls[21] since the vibrational motion perpendicular to the bond direction is also taken into account with the assumption of an isotropic system.[22]

In the analysis of the first-NN shell, the 24-K data were employed as an empirical standard. The first-NN distance at 24 K was assumed to be 4.00186 Å, given by x-ray diffraction.[18] The Fourier and fitting ranges were identical with the ones described above. Two different fitting methods were applied for the first-NN shell; one is the conventional harmonic (Gaussian) approximation (HA) for the radial distribution function ($\Delta C_3 = 0$ and $\Delta C_4 = 0$), and the other is the fourth-order cumulant-expansion (CE) formula.[8] The fitting parameters employed were $R_{\rm av}$ and ΔC_2 for the HA, and $R_{\rm av}$, ΔC_2, ΔC_3, and ΔC_4 for the CE formula since ΔE_0 and S_0^2 were assumed to be equal to those at 24 K. On the other hand, in the analysis of the third- and fourth-NN shells, only the HA method was applied, where the number of fitting parameters was 4 ($R_{\rm av}$ and ΔC_2 for each shell) and the ranges were again identical with the above ones. Note that

TABLE II. Structural parameters of solid Kr. For the first-NN distances, both values obtained by the fourth-order cumulant-expansion (CE) method and the harmonic approximation (HA) are given. Four details, see the text. All the errors estimated for data and fits correspond to the relative ones with respect to the lowest-temperature data.

		Distance (Å)					
Shell	T (K)	X-ray	CE	HA	ΔC_2 (10^{-2} Å^2)	ΔC_3 (10^{-3} Å^3)	ΔC_4 (10^{-4} Å^4)
First	24	4.0019	(4.002)	(4.002)	(0.00)	(0.00)	(0.00)
	25	4.0026	4.004(5)	4.002(5)	0.05(5)	0.05(1)	0.00(2)
	29	4.0055	4.006(5)	3.996(5)	0.26(5)	0.14(2)	0.06(2)
	35	4.0106	4.011(5)	3.996(5)	0.54(7)	0.29(4)	0.29(7)
	38	4.0133	4.015(5)	3.995(5)	0.74(10)	0.44(6)	0.48(10)
	43	4.0182	4.020(5)	3.990(5)	0.91(10)	0.70(10)	0.38(10)
Third	24	6.9314		(6.931)	(0.00)		
	25	6.9326		6.935(10)	0.08(10)		
	29	6.9378		6.940(10)	0.36(10)		
	35	6.9465		6.951(10)	0.74(15)		
	38	6.9513		6.956(10)	0.93(20)		
	43	6.9598		6.963(10)	1.22(20)		
Fourth	24	8.0037		(8.004)	(0.00)		
	25	8.0051		8.007(10)	0.04(10)		
	29	8.0111		8.012(10)	0.42(10)		
	35	8.0211		8.022(10)	0.75(15)		
	38	8.0266		8.020(10)	1.07(20)		
	43	8.0365		8.027(10)	1.43(20)		

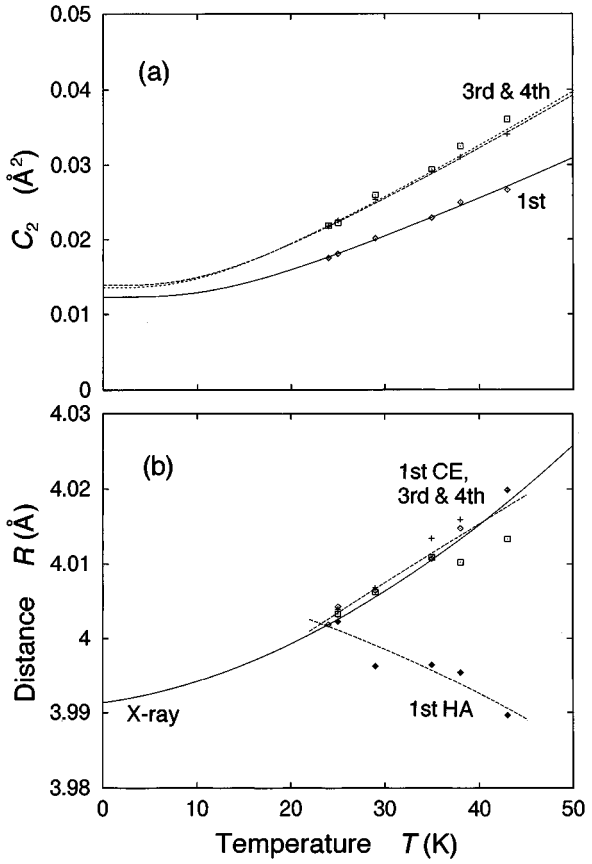

FIG. 3. Temperature dependence of (a) the mean-square relative displacements C_2 and (b) the average interatomic distances R_{av}. The EXAFS results are given as points. For C_2, the curves evaluated by the correlated Debye model assuming $\Theta_D = 61$ K are depicted for the first-NN (solid line), third-NN (long-dashed line), and fourth-NN (short-dashed line) shells. For the distance, the x-ray data (Ref. 18) are plotted as a solid line. The first-NN shell was analyzed in two different manners of the fourth-order cumulant-expansion formula (first CE, denoted as ◇) and the conventional harmonic (Gaussian) approximation (first HA, denoted as ◆). The third-NN (denoted as +) and fourth-NN (denoted as □) shells were analyzed only by the harmonic approximation, and these distances are scaled by factors of $1/\sqrt{3}$ and 0.5, respectively. Error bars are omitted to avoid complexity (see Table II).

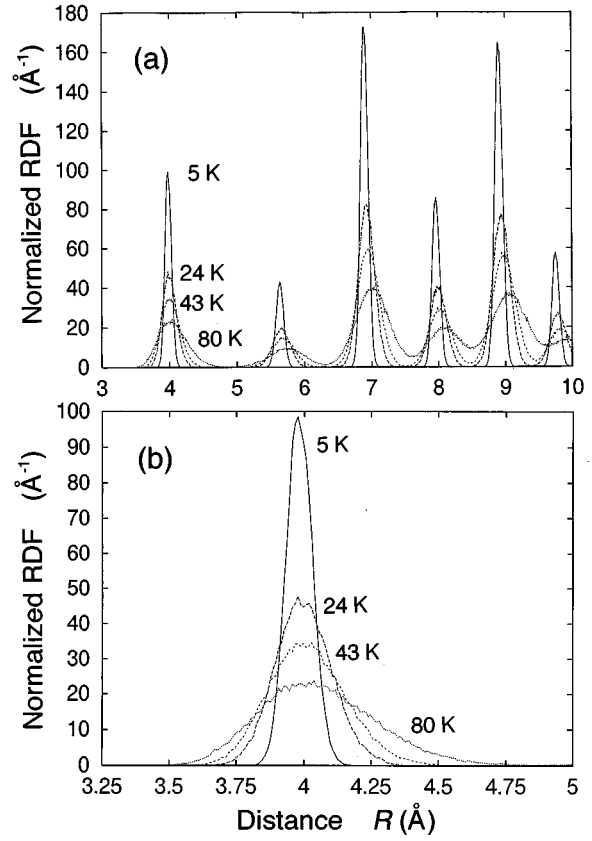

FIG. 4. Radial distribution functions $\rho(R)$ of solid Kr with respect to the central Kr atom, obtained with the MC simulations for the temperatures of 5, 24, 43, and 80 K. (b) corresponds to those for the first-NN shell.

although we have employed different ΔE_0 and S_0^2 values for each shell (see the above section), no temperature dependence of ΔE_0 and S_0^2 was assumed in order to suppress resultant uncertainties for C_2 and C_3.

The analysis results are shown in Table II and Fig. 3. For the first-NN C_2, only the CE results are given. From the temperature difference of C_2 for each shell, the Debye temperature Θ_D can be determined by assuming the correlated Debye model.[19] The first-NN analysis consequently yielded $\Theta_D = 61 \pm 2$ K [see Fig. 3(a)], which is also consistent with those estimated from the third- and fourth-NN shells. Note that all the curves given by the correlated Debye model were obtained with $\Theta_D = 61$ K. In Fig. 3, the absolute values of experimental C_2 at 24 K were assumed to be the ones evaluated by using the Debye model. The estimated Debye temperature of $\Theta_D = 61$ K is in good agreement with the calorimetric value of $\Theta_D = 62$ K (around 15 K, while at the $T \rightarrow 0$ limit $\Theta_D = 71.9$ K) (Ref. 23) and also with the x-ray diffraction data of $\Theta_D = 63$ K.[24]

The temperature dependence of the interatomic distance is subsequently discussed. In the case of the first-NN shell, the two different analysis methods (HA and CE) were employed and are found to provide noticeably different interatomic distances as seen in Table II and Fig. 3. The HA method gives apparent contraction of the interatomic distance with a temperature rise. This effect is well known[12] and implies the importance of the asymmetric distribution due to anharmonic vibration. When the fourth-order cumulant-expansion method was applied (the third-order expansion is sufficient for the distance estimation), such an apparent contraction was not observed and the resultant distance is well consistent with that determined by the x-ray diffraction.

In contrast, the HA analysis for the third- and fourth-NN shells yielded the proper temperature dependence of the interatomic distance as found in Table II and Fig. 3. In Fig. 3, these distances were scaled by factors of $1/\sqrt{3}$ and 0.5 for the third- and fourth-NN shells, respectively, to match the first-NN distance. Such an appropriate estimations for higher-NN distances should result from negligibly small values of C_3. Effective cancellation of the asymmetric contribution in the radial distribution function is thus experimentally clarified for higher-NN shells. It should also be noted that the thermal expansions using the average distances for all the shells are consistent with those estimated from the

TABLE III. Distances and cumulants at 5, 24, and 43 K, estimated from the MC simulations. R_{av} denotes the average distance, and R_{max} corresponds to the peak distance of the radial distribution function.

Shell	T (K)	R_{av} (Å)	R_{max} (Å)	C_2 (10^{-2} Å^2)	C_3 (10^{-3} Å^3)
First	5	3.9834	3.9753	0.238	0.014
	24	(4.0019)	3.9936	1.095	0.224
	43	4.0168	4.0013	2.026	0.812
Second	5	5.6337	5.6352	0.341	−0.004
	24	5.6556	5.6551	1.591	−0.104
	43	5.6798	5.6846	2.960	−0.287
Third	5	6.8969	6.8967	0.309	−0.001
	24	6.9265	6.9265	1.428	0.062
	43	6.9511	6.9492	2.704	0.106
Fourth	5	7.9646	7.9641	0.317	0.005
	24	7.9977	7.9963	1.472	0.056
	43	8.0255	8.0247	2.712	0.088

x-ray diffraction. This implies that local thermal expansion is identical with the long-range one within the present experimental accuracy.

IV. MONTE CARLO SIMULATIONS

A. Method

Di Cicco *et al.*[13] have performed the classical MC simulations of solid and liquid Kr under high pressure at room temperature. The present MC simulations have been carried out in a similar manner. Since the calculations are based on classical mechanics, it is difficult to provide quantitative information on vibrational properties at low temperature because of the zero-point vibration. Qualitative trends can, nevertheless, be discussed especially for thermal expansion. This is because the temperature range examined experimentally (24–43 K) is not so low for the quantum effect on thermal expansion to play a significant role, while the absolute vibrational amplitude C_2 is greatly affected by the zero-point vibration (see also below).

The closed-system, constant-pressure, and constant-temperature (N-P-T) MC simulations were examined at the temperatures of $T=5$, 24, 43, and 80 K and the pressure of $P=0$ Pa. The basic cell employed contains 256 atoms (4^3 fcc unit cells), and three-dimensional periodicity was imposed. The two-body Kr-Kr interatomic potential employed was the one proposed by Barker *et al.*[25] Although Di Cicco *et al.*[13] mentioned that the repulsive region of the potential does not fit the high-pressure EXAFS spectra, this effect was negligibly small for the present low-temperature data under vacuum. In each MC step, randomly chosen Kr atoms were tried to be displaced for 256 times (maximum displacement of 0.1 Å) and the lattice constant was possibly varied once (maximum variation of 0.01 Å). After sufficient equilibration, 10 000 MC steps were conducted to obtain the radial distribution function around the central Kr atom. The equilibrium first-NN distance at 24 K was resultantly obtained to be 3.9601 Å, which is shorter than the literature value of 4.001 86 Å.[18] In order to perform easier comparisons for temperature-dependent properties, all the distance quantities given by the MC simulations were multiplied by a factor of 1.0105.

B. Results

The radial distribution functions $\rho(R)$ (R is the distance with respect to the central Kr atom) obtained are shown in Fig. 4. Here $\rho(R)$ implies the probability for the presence of atoms in the range of $R\sim R+dR$; thus, the integration of $\rho(R)$ for the range of the shell of interest directly leads to the coordination number N. The first-, second-, third-, and fourth-NN shells appear at $\sim$4.0, $\sim$5.7, $\sim$6.9, and $\sim$8.0 Å, respectively. This confirms the fcc structure of simulated solid Kr. It is clear that with a temperature rise all the contributions are broadened and the peak positions for the higher-NN shells are shifted to longer distance sides.

TABLE IV. Thermal expansion of solid Kr estimated from the MC simulations. The x-ray values (Ref. 18) are also given for comparison.

	$(R_{av}-R_0)/R_0$ (10^{-3})				$(R_{max}-R_0)/R_0$ (10^{-3})			
Remark	5 K	24 K	43 K	80 K	5 K	24 K	43 K	80 K
X-ray	−2.4	(0.0)	4.1	15.9				
Lattice	−3.9	(0.0)	3.5	13.1	−3.9	0.1	3.6	13.0
First	−3.5	1.1	4.8	17.0	−5.5	−1.0	1.0	4.7
Second	−3.5	0.4	4.7	13.5	−3.2	0.3	5.5	15.7
Third	−3.9	0.4	3.9	13.6	−3.9	0.4	3.7	13.0
Fourth	−3.8	0.4	3.8	12.4	−3.9	0.2	3.7	12.5

Figure 4(b) describes the first-NN shell; the distribution function is clearly getting more asymmetric as temperature increases.

Table III summarizes the average distance R_{av}, the mode distance R_{max} (peak position of the radial distribution function), C_2, and C_3 for the first- to fourth-NN shells. The C_2 values for higher-NN shells are larger than those for the first-NN shell at any temperature. On the contrary, the C_3 values are found to be much larger in the first-NN shell than those in higher-NN shells. Although negative values of C_3 for the second-NN shell are not well understood, it should be noted that all the C_3 values for higher-NN shells are much smaller than those for the first-NN shell in spite of larger C_2.

Table IV tabulates the thermal expansion estimated by the MC simulations. Here the thermal expansion is defined using two different manners as $(R_{av}-R_0)/R_0$ and $(R_{max}-R_0)/R_0$, where R_0 is temperature independent and is assumed from the lattice constant at 24 K. The thermal expansion was separately estimated from the first- to fourth-NN shells. For comparison, the x-ray data[18] are also shown. The thermal expansions of the lattice constant estimated by the present MC simulations are found to be in good agreement with the x-ray diffraction data. A small discrepancy at 5 K should originate from the quantum effect of the thermal expansion; in a classical limit, the thermal expansion is proportional to absolute temperature T, while in the quantum-mechanical theory the thermal expansion is getting smaller with a temperature decrease and converges to a certain constant at the $T\rightarrow 0$ limit.[3,5–7,9]

The thermal expansions using the average distances for all the shells are consistent with those estimated from the lattice constant, this being consistent with the above EXAFS results. The thermal expansion estimated from the mode distance R_{max} for the first-NN shell is noticeably smaller than that from the lattice constant because of the anharmonicity of the interatomic potential. On the other hand, those for higher-NN shells are in good accordance with the ones from the lattice constant. These findings are essentially consistent with the present EXAFS results and the remark given by Di Cicco *et al.*,[13] and confirm that the asymmetric distribution resulted from the potential anharmonicity should effectively be compensated in the higher-NN shells.

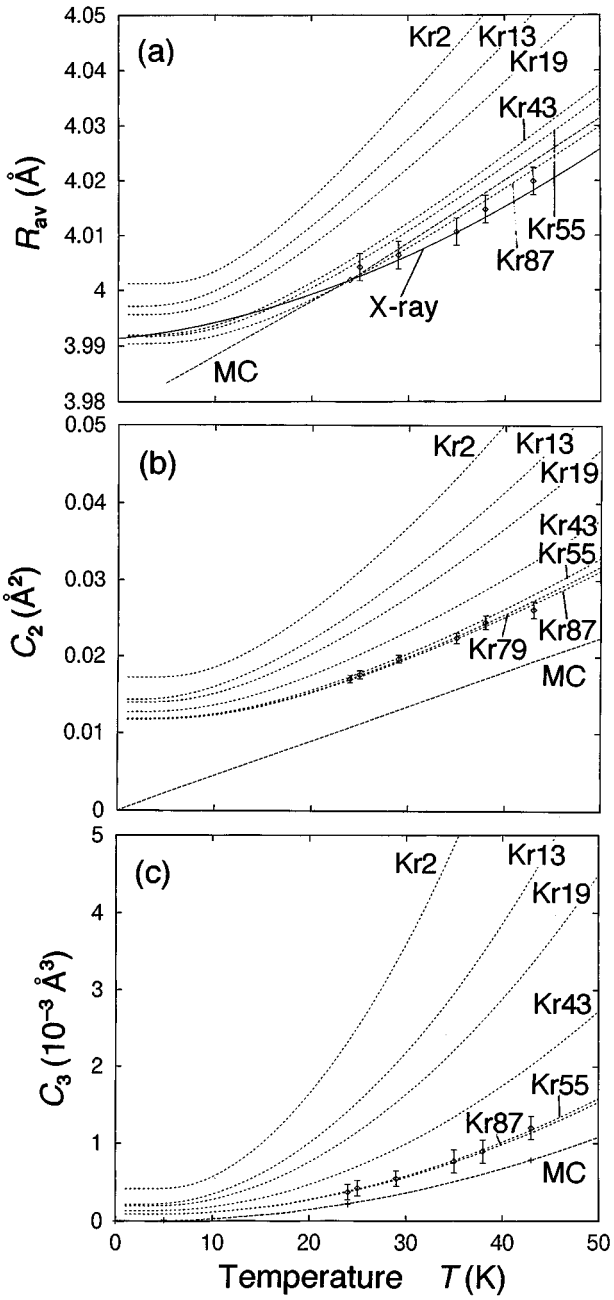

FIG. 5. Temperature dependence of (a) the average interatomic distances R_{av}, (b) mean-square relative displacements C_2, and (c) the mean-cubic relative displacements C_3 for the first-NN Kr-Kr shell estimated by the quantum-statistical calculations of the Kr_2, Kr_{13}, Kr_{19}, Kr_{43}, Kr_{55}, Kr_{79}, and Kr_{87} clusters (short-dashed lines). The results of the classical MC simulations of solid Kr (long-dashed line) are also given, together with the EXAFS results (points with error bars) and the x-ray diffraction data (solid line) for R_{av}. The results of R_{av} and C_3 for Kr_{79} are omitted because these are almost identical with those of Kr_{87}.

V. QUANTUM-STATISTICAL CALCULATION

A. Method

In order to discuss the thermal properties of solids at low temperature, the quantum effect might be important, which has not been taken into account in the previous section. We have performed in the present study the quantum-statistical calculations of the EXAFS cumulants of Kr clusters. We will here employ the same adiabatic pair potential as the classical MC simulations. The pair potential $v(r)$ can be expanded around the potential minimum r_0 as the fourth-order polynomial:

$$v(r)=\tfrac{1}{2}\kappa_0(r-r_0)^2-\kappa_3(r-r_0)^3+\kappa_4(r-r_0)^4, \qquad (2)$$

where κ_0, κ_3, and κ_4 are the second-, third-, and fourth-order force constants. The linear least-squares fit of the original potential given by Barker *et al.*[25] worked quite well, and the resultant values are $\kappa_0=0.014\,86$ (mdyn/Å), $\kappa_3=0.011\,37$ (mdyn/Å^2), $\kappa_4=0.006\,255$ (mdyn/Å^3), and $r_0=4.007\,87$ (Å), respectively. For a following use of the pair potential, however, it would be better to expand the function with respect to the average distance R_{av} instead of r_0 due to

its more accuracy in the perturbation calculations.[3] Thus the pair potential is rewritten as

$$v(r)=\tfrac{1}{2}\kappa_0'(r-R_{\rm av})^2+\kappa_1'(r-R_{\rm av})-\kappa_3'(r-R_{\rm av})^3 +\kappa_4(r-R_{\rm av})^4+v(R_{\rm av}), \tag{3}$$

where modified force constants can easily be obtained by comparing Eqs. (2) and (3), namely,

$$\kappa_0'=\kappa_0-6\kappa_3C_1+12\kappa_4C_1,$$
$$\kappa_1'=\kappa_0C_1-3\kappa_3C_1^2+4\kappa_4C_1^3,$$
$$\kappa_3'=\kappa_3-4\kappa_4C_1, \tag{4}$$

where $C_1=R_{\rm av}-r_0$ describes the thermal expansion. Note that the adiabatic potential apparently contains a temperature-dependent quantities such as C_1.

Let us here assume that the total potential $V(r)$ of the Kr cluster can simply be given as a sum of the pair potential taking account of only the first-NN two-body interaction. When the first-, third-, and fourth-order potential terms are regarded as a perturbed Hamiltonian, a nonperturbed Schrödinger equation with the harmonic second-order potential is exactly solved. The total potential $V(r)$ is consequently expressed using the normal coordinates (nonperturbed eigenfunctions) $\mathbf{Q}$ as

$$V(r)=\sum_{i<j}^{\rm 1st\ NN} v_{ij}(r) =\frac{1}{2}\sum_p \omega_p^2Q_p^2+\sum_p \alpha_p^{(1)}Q_p-\sum_{p\le q\le r}\alpha_{pqr}^{(3)}Q_pQ_qQ_r +\sum_{p\le q\le r\le s}\alpha_{pqrs}^{(4)}Q_pQ_qQ_rQ_s, \tag{5}$$

where ω_p is the pth normal vibrational frequency associated with the normal coordinate Q_p. Here again note that ω_p and Q_p are slightly temperature dependent.

The thermal average of any physical quantity can be evaluated quantum statistically within the first-order perturbation theory using Eqs. (4)–(6) in Ref. 5. C_1 can be obtained by solving the following equation approximately:

$$0=\langle r-R_{\rm av}\rangle=\sum_i e_i^{(1)}\langle Q_i\rangle =\sum_i e_i^{(1)}\frac{2\sigma_i^2}{\hbar\omega_i}\left(-\alpha_i^{(1)}+3\sum_p \alpha_{ipp}^{(3)}\frac{1+z_p}{1-z_p}\right), \tag{6}$$

where $\mathbf{e}^{(1)}$ is the coefficients with which the normal coordinates are transformed into the initial internal coordinates, and the leading term of C_1 is included in $\alpha_i^{(1)}$. C_2 and C_3 are calculated as:

$$C_2=\sum_{i,j} e_{ij}^{(2)}\langle Q_iQ_j\rangle=\sum_i e_{ii}^{(2)}\sigma_i^2\frac{1+z_i}{1-z_i}-24\sum_{i,j} e_{ij}^{(2)}\sigma_i^2\sigma_j^4\left(\frac{1-z_iz_j}{\hbar(\omega_i+\omega_j)}+\frac{z_i-z_j}{\hbar(-\omega_i+\omega_j)}\right)\frac{1}{1-z_i}\frac{1+z_j}{1-z_j}\sum_p \alpha_{ijpp}^{(4)}\sigma_p^2\frac{1+z_p}{1-z_p}, \tag{7}$$

$$C_3=\sum_{i,j,k} e_{ijk}^{(3)}\langle Q_iQ_jQ_k\rangle-3C_1C_2 =12\sum_{i,j,k}\frac{e_{ijk}^{(3)}\alpha_{ijk}^{(3)}\sigma_i^2\sigma_j^2\sigma_k^2}{(1-z_i)(1-z_j)(1-z_k)}\left(\frac{1-z_iz_jz_k}{\hbar(\omega_i+\omega_j+\omega_k)}+\frac{z_k-z_iz_j}{\hbar(\omega_i+\omega_j-\omega_k)}+\frac{z_j-z_iz_k}{\hbar(\omega_i-\omega_j+\omega_k)}+\frac{z_i-z_jz_k}{\hbar(-\omega_i+\omega_j+\omega_k)}\right). \tag{8}$$

Note that the subscripts of the force constants are mutable; for instance, $\alpha_{jik}^{(3)}=\alpha_{ijk}^{(3)}$, $\alpha_{jikl}^{(4)}=\alpha_{ijkl}^{(4)}$, and so forth. C_4 can also be given in a similar manner to C_3.

In the present study, we have examined several sizes of Kr clusters of Kr_2, Kr_3 (linear), Kr_5 (planar), Kr_{13} (including all the first-NN atoms), Kr_{19} (up to the second NN), Kr_{43} (up to the third), Kr_{55} (up to the fourth), Kr_{79} (up to the fifth), and Kr_{87} (up to sixth). In the Kr_{55} cluster, all the first-NN atoms are coordinated completely by 12 atoms. We will hereafter discuss the results only of the first-NN shell because of a limited size of the present cluster and a neglect of higher-NN interaction. Note that no fitting parameters with the experiments are included in the following results except for the absolute values of $R_{\rm av}$, C_2, and C_3 at 24 K.

B. Results

Figure 5 shows the calculated results of $R_{\rm av}$, C_2, and C_3 for the first-NN shell of Kr_2, Kr_{13}, Kr_{19}, Kr_{43}, Kr_{55}, Kr_{79}, and Kr_{87}, together with the experimental and the above MC ones. The results of Kr_3 and Kr_5 are essentially the same as those of Kr_2 because of no interaction between the terminal Kr atoms, and $R_{\rm av}$ and C_3 of Kr_{79} are almost identical with those of Kr_{87}. These curves are thus omitted in Fig. 5. The calculated $R_{\rm av}$ at 24 K for the Kr_{87} cluster was obtained to be 4.0462 Å, which is significantly larger than the experimental value of 4.001 86 Å.[18] This deviation originates from the neglect of higher-NN attractive interactions. Here the calculated $R_{\rm av}$ values by both quantum-statistic (Kr_{87}) and classical MC methods were thus shifted by adding constants to match the experimental value at 24 K. On the other hand, C_2 and C_3 were similarly shifted to match the calculated ones at 24 K for Kr_{87}.

It is clearly found that the temperature dependence of all the quantities is getting smaller with an increase in the cluster size. This is because the neighboring atoms are gradually more coordinated and the vibrational amplitude becomes

suppressed. Although the temperature dependence does not converge within the cluster size investigated, the Kr_{87} cluster may be sufficiently large to discuss the EXAFS cumulants of the first-NN shell. We should here note that when the diatomic Einstein model is applied to obtain the force constants of solids, the resultant values should be just effective and completely different from those of the pair potential.

The thermal expansion estimated by the present quantum-statistical calculation for Kr_{55} is found to be in excellent agreement with those given by EXAFS, x-ray diffraction, and the classical MC simulations [Fig. 5(a)]. This implies reliability of the present pair potential employed and confirms appropriate estimation of thermal expansion using the classical theory at the temperature range investigated. At lower temperatures, the classical calculation deviates from the experiments, while the quantum-statistical results agrees with those fairly well.

C_2 and C_3 were also estimated appropriately by the quantum-statistical calculations [Figs. 5(b) and 5(c)]. The temperature dependence of C_2 and C_3 is reproduced excellently by the calculations of Kr_{79} and Kr_{87}. Even in the case of Kr_{43} (or also of Kr_{55} for C_2), the temperature dependence was significantly overestimated. On the other hand, the classical C_2 deviates noticeably from the experimental data because of the quantum effect of the zero-point vibration, while the slope of the classical C_2 is in good accordance with the experiments, again indicating that the temperature examined in this study is not crucially too low to obtain thermal information of solid Kr by means of the classical theory.

VI. CONCLUSIONS

The Kr K-edge EXAFS spectra of solid Kr were measured and analyzed in order to obtain information on the thermal expansion and the Debye temperature not only from the first-NN shell, but from higher-NN shells. The mean-square relative displacements for the third- and fourth-NN shells were found to be larger than those for the first-NN shell. All the shells yielded the Debye temperature of 61 ± 2 K. The thermal expansion estimated from the first-, third-, and fourth-NN shells are in excellent agreement with the x-ray data. For the first-NN shell, the cumulant-expansion analysis was essentially important, while for the third- and fourth-NN shells, the conventional Gaussian approximation successfully gives the proper thermal expansion. Effective cancellation of anharmonicity should be emphasized in the radial distribution function for higher-NN shells, although the present system is largely disordered.

We have also performed the classical NPT MC simulations of solid Kr at low temperature in order to recognize the behaviors of the temperature dependence of the EXAFS cumulants and the lattice constant. Although the simulation was based on the classical statistics, these behaviors were successfully reproduced at least semiquantitatively. The mean-square relative displacements are larger for higher-NN shells than for the first-NN shell because of larger correlated motions for the latter. On the contrary, the mean-cubic relative displacements were revealed to be negligibly small for higher-NN shells, while those for the first-NN shell are essentially important to estimate an appropriate average interatomic distance.

The present findings should be applicable to other systems for more reliable estimation of the interatomic distance by means of EXAFS. It might be believed that the first-NN shell is most reliable for a detailed determination of the interatomic distance owing to dominant contribution in the EXAFS spectra. It is, however, quite important to take the anharmonic contribution into account; otherwise, an apparent contraction of the bond length should be inevitable.[12] On the other hand, when higher-NN shells are observed, reliable interatomic distances are obtainable within the Gaussian approximation even in strongly anharmonic materials. Although the present study employed two-body interatomic potentials, this finding can be applied to the systems with strong many-body interactions such as a bending force. This is because, as long as the interatomic distance is discussed, the bending anharmonicity for the distance is always canceled.[7] Care should be taken only of higher-order cumulants such as C_3.

The quantum-statistical analytical calculations of the first-NN cumulants using the Kr_{87} cluster were found to be in excellent agreement with the experimental results. This implies a high quality of the pair potential employed. We have examined the cluster-size dependence of the EXAFS cumulants from Kr_2 to Kr_{87} and have found that temperature dependence of R_{av}, C_2, and C_3 is noticeably suppressed with an increase in the cluster size. This is because the first-NN atoms are gradually more frozen due to further coordination of Kr atoms. It should be noted that the diatomic Einstein model, if applied, would result in only an effective potential of solid Kr, which completely deviates from the intrinsic pair potential. The present quantum-statistical calculations have dealt with only the first-NN shell and ignored higher-NN interactions. It might be also important to evaluate the cumulants of higher-NN shells by modifying the theory derived by Fujikawa and Miyanaga,[10,11] for further understanding of thermal expansion and effective cancellation of asymmetric distributions for higher-NN shells.

ACKNOWLEDGMENTS

The present authors gratefully acknowledge Dr. I. Ono and K. Kaneyuki for their contribution to the EXAFS measurements and analysis. We are also grateful to Professor M. Nomura of the Photon Factory. This work has been carried out under the approval of Photon factory Program Advisory Committee (PF-PAC No. 91-188).

[1] T. Yokoyama, T. Satsukawa, and T. Ohta, Jpn. J. Appl. Phys. **28**, 1905 (1989).
[2] T. Yokoyama and T. Ohta, Jpn. J. Appl. Phys. **29**, 2052 (1990).
[3] A. I. Frenkel and J. J. Rehr, Phys. Rev. B **48**, 585 (1993).
[4] L. Tröger, T. Yokoyama, D. Arvanitis, T. Lederer, M. Tischer, and K. Baberschke, Phys. Rev. B **49**, 888 (1994).
[5] T. Yokoyama, K. Kobayashi, T. Ohta, and A. Ugawa, Phys. Rev. B **53**, 6111 (1996).
[6] T. Yokoyama, Y. Yonamoto, and T. Ohta, J. Phys. Soc. Jpn. **65**, 3901 (1996).

[7] T. Yokoyama, Y. Yonamoto, T. Ohta, and A. Ugawa, Phys. Rev. B **54**, 6921 (1996).
[8] G. Bunker, Nucl. Instrum. Methods **207**, 437 (1983).
[9] H. Rabus, Ph.D. thesis, Department of Physics, Freie Universität Berlin, 1991.
[10] T. Fujikawa and T. Miyanaga, J. Phys. Soc. Jpn. **62**, 4108 (1993).
[11] T. Miyanaga and T. Fujikawa, J. Phys. Soc. Jpn. **63**, 1036 (1994).
[12] P. Eisenberger and G. S. Brown, Solid State Commun. **29**, 481 (1979).
[13] A. Di Cicco, A. Filipponi, J. P. Itié, and A. Polan, Phys. Rev. B **54**, 9086 (1996).
[14] H. Oyanagi, T. Matsushita, M. Ito, and H. Kuroda (unpublished); M. Nomura (unpublished); M. Nomura and A. Koyama (unpublished).
[15] See, for instance, *X-ray Absorption: Principles, Applications, Techniques of EXAFS, SEXAFS and XANES*, edited by D. C. Koningsberger and R. Prins (Wiley, New York, 1988).
[16] T. Yokoyama, H. Hamamatsu, and T. Ohta, Computer code EXAFSH, version 2.1, The University of Tokyo, 1993.
[17] S. I. Zabinsky, J. J. Rehr, A. Ankudinov, R. C. Albers, and M. J. Eller, Phys. Rev. B **52**, 2995 (1995).
[18] *Thermodynamical Properties of Matter*, edited by Y. S. Touloukian, R. K. Kirby, R. E. Taylor, and T. Y. R. Lee (Plenum, New York, 1975), Vol. 13; G. K. Horton, Am. J. Phys. **36**, 93 (1968).
[19] G. Beni and P. M. Platzman, Phys. Rev. B **14**, 1514 (1976).
[20] B. K. Teo, J. Am. Chem. Soc. **103**, 3990 (1981); N. Alberding and E. D. Crozier, in *EXAFS and Near Edge Structure III*, edited by K. O. Hodgson, B. Hedman, and J. E. Penner-Hahn, Springer Proceedings in Physics Vol. 2 (Springer, Berlin, 1984), p. 30; A. Filipponi and A. Di Cicco, Phys. Rev. B **52**, 15 135 (1995).
[21] J. M. Tranquada and R. Ingalls, Phys. Rev. B **28**, 3520 (1983).
[22] T. Ishii, J. Phys. C **4**, 8029 (1992); E. A. Stern (unpublished).
[23] L. Finegold and N. E. Phillips, Phys. Rev. **177**, 1383 (1969).
[24] *International Tables for X-ray Crystallography*, edited by C. H. Macgillavry, G. D. Rieck, and K. Lonsdale (Kynoch, Birmingham, 1962), Vol. III, p. 234.
[25] J. A. Barker, R. O. Watts, J. K. Lee, T. P. Schafer, and Y. T. Lee, J. Chem. Phys. **61**, 3081 (1974).